NASA TM X-427

TECHNICAL MEMORANDUM

X-427

AN INVESTIGATION OF THE INFLUENCE OF BODY SIZE AND INDENTATION ASYMMETRY ON THE EFFECTIVENESS OF BODY INDENTATION IN COMBINATION WITH A CAMBERED WING

By James C. Patterson, Jr., and
Donald L. Loving

Langley Research Center
Langley Field, Va.

Declassified March 15, 1962

NATIONAL AERONAUTICS AND SPACE ADMINISTRATION
WASHINGTON

February 1961

NATIONAL AERONAUTICS AND SPACE ADMINISTRATION

TECHNICAL MEMORANDUM X-427

AN INVESTIGATION OF THE INFLUENCE OF BODY SIZE AND INDENTATION ASYMMETRY ON THE EFFECTIVENESS OF BODY INDENTATION IN COMBINATION WITH A CAMBERED WING*

By James C. Patterson, Jr., and
Donald L. Loving

SUMMARY

An investigation has been made of a 45° sweptback cambered wing in combination with an unindented body and a body symmetrically indented with respect to its axes designed for a Mach number of 1.2. The ratio of body frontal area to wing planform area was 0.08 for these wing-body combinations. In order to determine the influence of body size on the effectiveness of indentation, the test data have been compared with previously obtained data for similar configurations having a ratio of body frontal area to wing planform area of 0.04. Also, in order to investigate the relative effectiveness of indentation asymmetry, a specially indented body designed to account for the wing camber and also designed for a Mach number of 1.2 has been included in these tests. The investigation was conducted in the Langley 8-Foot Tunnels Branch at Mach numbers from 0.80 to 1.43 and a Reynolds number of approximately 1.85×10^6, based on a mean aerodynamic chord length of 5.955 inches.

The data indicate that the configurations with larger ratio of body frontal area to wing planform area had smaller reductions in zero-lift wave drag associated with body indentation than the configurations with smaller ratio of body frontal area to wing planform area. The 0.08-area-ratio configurations also had correspondingly smaller increases in the values of maximum lift-drag ratio than the 0.04-area-ratio configurations. The consideration of wing camber in the body indentation design resulted in a 35.5-percent reduction in zero-lift wave drag, compared with a 21.5-percent reduction associated with the symmetrical indentation, but had a negligible effect on the values of maximum lift-drag ratio.

*Title, Unclassified.

INTRODUCTION

A number of investigations of the area rule have revealed that body indentation produces a favorable reduction in zero-lift wave drag. Examples of such investigations are found in references 1 and 2. Little information, however, is available on the effect of body size on the effectiveness of body indentation. In order to determine the influence of body size on indentation effectiveness, an investigation of the aerodynamic characteristics of a wing-body combination having a ratio of body frontal area to wing planform area of 0.08 has been conducted. This investigation is a continuation of the investigation of reference 2, where similar configurations were tested with a ratio of body frontal area to wing planform area of 0.04.

It has been suggested in reference 3 that an improvement in the effectiveness of body indentation may be obtained by considering the wing cross-sectional area above and below the chord plane separately. An asymmetrically indented body, therefore, designed to account for the camber of the wing also has been investigated.

The tests were made in the Langley 8-Foot Tunnels Branch at Mach numbers from 0.80 to 1.43 and an average Reynolds number of 1.85×10^6.

SYMBOLS

a	mean-line designation, fraction of chord from leading edge over which design load is uniform
A_B	body frontal area
b	wing span
c	wing chord measured parallel to plane of symmetry
$\bar{c}$	mean aerodynamic chord, $\frac{2}{S_w}\int_0^{b/2} c^2 dy$
C_D	drag coefficient, $\frac{\text{Drag}}{qS_w}$
$C_{D,o}$	zero-lift drag coefficient, $\frac{\text{Zero-lift drag}}{qS_w}$

$\Delta C_{D,o}$ zero-lift wave-drag coefficient, $(C_{D,o})_M - (C_{D,o})_{M=0.8}$

C_L lift coefficient, $\frac{\text{Lift}}{qS_w}$

$\frac{\partial C_L}{\partial \alpha}$ lift-curve slope, averaged over a lift-coefficient range from -0.05 to 0.3

C_m pitching-moment coefficient about 25 percent chord of mean aerodynamic chord, $\frac{\text{Pitching moment}}{qS_w\bar{c}}$

$\frac{\partial C_m}{\partial C_L}$ static-longitudinal-stability parameter averaged over a lift-coefficient range from -0.05 to 0.3

D_{max} maximum diameter of basic body

$(L/D)_{max}$ maximum lift-drag ratio

M Mach number

q free-stream dynamic pressure, $\frac{1}{2}\rho V^2$

S_w total wing planform area

V velocity of undisturbed stream

x body station, distance from nose of body

y coordinate along span

α angle of attack of body center line

ρ mass density in undisturbed stream

θ cutting-plane roll angle, deg

MODELS AND APPARATUS

Geometric characteristics of the wing-body combinations used in this investigation are shown in figure 1. A photograph of one of the models in the Langley 8-foot transonic pressure tunnel is shown as figure 2. The stainless-steel cambered wing of the present investigation

has a planform area equal to one-half the wing planform area of reference 2. The models of reference 2 had a ratio of body frontal area to wing planform area A_B/S_W of 0.04; whereas for the present investigation, that ratio is 0.08. With this exception, the wings are the same and have an aspect ratio of 4, a taper ratio of 0.15, and 45° sweepback of the quarter-chord line. At the wing root, an NACA 64A206, a = 0 airfoil section (measured streamwise) is used. An NACA 64A203, a = 0.8 (modified) airfoil section is used from the midsemispan of the wing to the tip. Straight-line elements were used in fairing the wing sections from the root to midsemispan. The present wing is mounted in a midwing position on a sting-supported body for all test configurations and is located longitudinally on the body such that the leading edge of the mean aerodynamic chord is at the same body station (17.895 inches) as that of reference 2. The airfoil ordinates at several stations along the wing semispan are given in table I.

Three bodies have been tested in combination with the cambered wing of this investigation. The first of these bodies, which is identical to the Sears-Haack body of reference 2, is unindented and is referred to as the basic body. A second body is designed for a Mach number of 1.2 by using the axially symmetrical indentation procedure of reference 1 and is referred to as the symmetrically indented body. A body axially symmetrically indented in the same manner is referred to as the M = 1.2 body in reference 2. This M = 1.2 body and the symmetrically indented body were obtained by indenting a modified body which has a diameter slightly larger than the basic body, as indicated in reference 2. A third body designed for a Mach number of 1.2 is indented to compensate for the camber of the wing. This body also was obtained by indenting the modified body and is referred to as the asymmetrically indented body. The upper half of the body is designed on the basis of the wing cross-sectional areas above the chord plane, while the indentation for the lower half of the body accounts for the areas below the chord plane in the manner suggested in reference 3. The volume of each of the indented bodies is about 95 percent of the volume of the basic body. Representative axial distribution of cross-sectional area for the configurations is shown in figures 3 and 4 for roll angles of 0°, 45°, and 90° at Mach numbers of 1.0, 1.2, and 1.4. Ordinates for all contours of the basic body, the modified body, the symmetrically indented body, and the asymmetrically indented body are given in table II.

TESTS

Each wing-body combination was tested at Mach numbers ranging from 0.80 to 1.43 at a tunnel stagnation pressure of 1 atmosphere. The

angle-of-attack range extended from -2° to 16°. All wing-body combinations were tested with transition fixed along the span of the wing at 10 percent of the local chord on both the upper and lower surfaces of the wing and around the nose of the model at 10 percent of the body length, as shown in figure 2. The transition strips are 0.10 inch wide and were formed by sprinkling No. 120 carborundum grains on a plastic adhesive. The basic and symmetrically indented body configurations were also tested with transition natural. For this investigation the average Reynolds number, based on the wing mean aerodynamic chord, was approximately 1.85×10^6.

MEASUREMENTS AND ACCURACY

Measurements of lift, drag, and pitching moment were obtained by the use of an internally mounted, sting-supported, strain-gage balance. The coefficients of these forces and moments are estimated to be accurate within the following limits: C_L, ± 0.01; $C_{D,o}$, ± 0.0005; and C_m, ± 0.004. These limits include the effect of possible errors in the measurements of the angle of attack and effects of wall reflections at a Mach number of 1.13. The force and moment results also have been adjusted to the condition of stream static pressure on the base of the body. The angle of attack was measured, with an accuracy of $\pm 0.10^{\circ}$, by a fixed-pendulum strain-gage unit mounted in the nose of the model.

RESULTS AND DISCUSSION

The basic data in the form of the variation of angle of attack, drag coefficient, and pitching-moment coefficient with lift coefficient are shown in figure 5 for the basic, symmetrically indented, and asymmetrically indented configurations with transition fixed and in figure 6 for the basic and symmetrically indented configurations with transition natural. Figures 7 to 13 are analysis figures and are based on transition-fixed data. In the analysis figures, the drag coefficients for the basic body configuration have been adjusted for volume in the manner described in reference 2.

Drag Characteristics

An increase in body size resulted in an increase in the values of the zero-lift wave-drag coefficient for the basic and symmetrically indented body configurations, as would be expected (fig. 7). The reduction of the zero-lift wave-drag coefficient associated with the

use of the symmetrically indented body configuration for the large ratio of body frontal area to wing area $\frac{A_B}{S_w} = 0.08$, at Mach numbers in the region of 1.2, was significantly less than that obtained by the M = 1.2 configuration $\left(\frac{A_B}{S_w} = 0.04\right)$ of reference 2. This trend is in agreement with calculations of wave-drag coefficients based on the method of reference 4. It should be noted that because the same size basic body was tested with both the larger wing of reference 2 and the smaller wing of this investigation, the body wave-drag contribution is twice as large when based on the smaller wing area.

The effectiveness of asymmetrical indentation on zero-lift wave-drag coefficient is compared with that of symmetrical indentation in figure 8. The values of zero-lift wave-drag coefficient associated with the symmetrically indented body of the present investigation were approximately 0.0019 lower than those for the basic body configuration in the indentation design Mach number range. The asymmetrically indented body reduced the zero-lift wave-drag coefficient $\Delta C_{D,o}$ by an additional amount of 0.0013. The zero-lift wave drag of the basic configuration was therefore reduced 35.5 percent for the asymmetrical indentation compared with 21.5 percent for the symmetrical indentation.

The increase in zero-lift wave drag associated with the increase in body size is reflected as a decrease in the value of maximum lift-drag ratio. This difference in the values of the maximum lift-drag ratio shown in figure 9 also is associated with the additional wetted area of the $\frac{A_B}{S_w} = 0.08$ configurations in comparison with that for the $\frac{A_B}{S_w} = 0.04$ configurations.

The maximum lift-drag ratios of the configurations with the symmetrically indented body and the asymmetrically indented body were approximately the same throughout the Mach number range (fig. 10). The lack of evidence in these $(L/D)_{max}$ values of the advantageous, though small, additional reduction in zero-lift wave drag associated with the asymmetrically indented body can be attributed to an increase in the drag due to lift that was obtained from this particular asymmetrical indentation.

Lift and Pitching-Moment Characteristics

The effects of body size and body indentation on the lift-curve slope, the pitching-moment characteristics, and the center-of-pressure

location throughout the Mach number range were not critical. (See figs. 11, 12, and 13, respectively.)

CONCLUSIONS

The results of this investigation to determine the influence of body size on the effectiveness of indentation and also to determine the effect of asymmetrically indenting a body to account for wing camber have indicated the following conclusions:

1. Smaller reductions occurred in the zero-lift wave drag associated with body indentation for the configurations with larger ratio of body frontal area to wing planform area than for the configurations with smaller ratio; analogously, smaller increases in the values of maximum lift-drag ratio were realized for the larger area-ratio configurations than for the smaller area-ratio configurations.

2. Asymmetrical indentation reduced the zero-lift wave drag of the basic configuration 35.5 percent whereas symmetrical indentation reduced the zero-lift wave drag 21.5 percent. The values of maximum lift-drag ratio, however, remained approximately the same for both the symmetrically and asymmetrically indented body configurations.

Langley Research Center,
National Aeronautics and Space Administration,
Langley Field, Va., September 19, 1960.

REFERENCES

1. Whitcomb, Richard T., and Fischetti, Thomas L.: Development of a Supersonic Area Rule and an Application to the Design of a Wing-Body Combination Having High Lift-to-Drag Ratios. NASA TR R-72, 1960. (Supersedes NACA RM L53H31a.)

2. Loving, Donald L.: A Transonic Investigation of Changing Indentation Design Mach Number on the Aerodynamic Characteristics of a 45° Sweptback-Wing—Body Combination Designed for High Performance. NACA RM L55J07, 1956.

3. Whitcomb, Richard T.: Some Considerations Regarding the Application of the Supersonic Area Rule to the Design of Airplane Fuselages. NACA RM L56E23a, 1956.

4. Holdaway, George H.: Comparison of Theoretical and Experimental Zero-Lift Drag-Rise Characteristics of Wing-Body-Tail Combinations Near the Speed of Sound. NACA RM A53H17, 1953.

TABLE I

AIRFOIL ORDINATES

Chord station, percent chord	Ordinate, percent chord									
	Root-chord station (c = 8.755 in.)		11.86-percent-semispan station (c = 7.872 in.)		23.72-percent-semispan station (c = 6.990 in.)		35.58-percent-semispan station (c = 6.107 in.)		50-percent-semispan to tip stations (c = 5.03- in. at midsemispan; c = 1.313 in. at tip)	
	Upper surface	Lower surface	Upper surface	Lower surface	Upper surface	Lower surface	Upper surface	Lower surface	Upper surface	Lower surface
0	0	0	0	0	0	0	0	0	0	0
.25	.47	-.25	.43	-.23	.38	-.21	.32	-.19	.21	-.13
.5	.62	-.36	.57	-.33	.52	-.30	.44	-.25	.31	-.18
.75	.75	-.43	.69	-.40	.62	-.35	.53	-.30	.38	-.21
1.25	.96	-.53	.89	-.48	.80	-.43	.68	-.36	.49	-.25
2.5	1.37	-.67	1.28	-.62	1.15	-.55	1.00	-.45	.72	-.30
5	1.95	-.85	1.82	-.77	1.65	-.68	1.44	-.54	1.07	-.34
10	2.76	-1.08	2.58	-.97	2.36	-.84	2.06	-.66	1.56	-.36
15	3.31	-1.25	3.11	-1.12	2.84	-.95	2.50	-.73	1.92	-.36
20	3.71	-1.41	3.48	-1.25	3.20	-1.04	2.84	-.79	2.20	-.35
30	4.15	-1.64	3.92	-1.44	3.62	-1.18	3.24	-.86	2.60	-.30
40	4.23	-1.77	4.01	-1.54	3.73	-1.24	3.38	-.87	2.78	-.22
50	3.93	-1.72	3.75	-1.47	3.52	-1.16	3.23	-.76	2.74	-.08
60	3.36	-1.52	3.23	-1.28	3.07	-.97	2.87	-.58	2.52	.08
70	2.60	-1.22	2.53	-1.00	2.44	-.72	2.33	-.37	2.14	.22
80	1.73	-.84	1.71	-.67	1.68	-.46	1.64	-.17	1.57	.30
90	.85	-.45	.84	-.35	.84	-.23	.83	-.09	.82	.17
100	.01	-.01	.01	-.01	.01	-.01	.01	-.01	.01	-.01

TABLE II

BODY ORDINATES

Forebody	
Body station, in.	Radius, in.
0	0
.5	.165
1.0	.282
1.5	.378
2.0	.460
2.5	.540
3.0	.612
3.5	.680
4.0	.743
4.5	.806
5.0	.862
5.5	.917
6.0	.969
6.5	1.015
7.0	1.062
7.5	1.106
8.0	1.150
8.5	1.187
9.0	1.222
9.5	1.257
10.0	1.290
10.5	1.320
11.0	1.350
11.5	1.376
12.0	1.404

Afterbody					
Body station, in.	Radius, in., for -				
	Basic body	Modified body	Symmetrically indented body	Asymmetrically indented body	
				Upper	Lower
12.5	1.430	1.430	1.430	1.430	1.430
13.0	1.452	1.454	1.454	1.452	1.452
13.5	1.476	1.477	1.477	1.476	1.476
14.0	1.493	1.499	1.499	1.499	1.499
14.5	1.512	1.520	1.519	1.519	1.519
15.0	1.526	1.540	1.530	1.526	1.534
15.5	1.540	1.558	1.533	1.522	1.544
16.0	1.552	1.575	1.530	1.513	1.550
16.5	1.565	1.590	1.520	1.484	1.553
17.0	1.575	1.604	1.507	1.455	1.553
17.5	1.585	1.615	1.493	1.427	1.553
18.0	1.590	1.626	1.480	1.397	1.553
18.5	1.598	1.634	1.471	1.373	1.552
19.0	1.602	1.642	1.466	1.369	1.553
19.5	1.606	1.646	1.467	1.370	1.554
20.0	1.606	1.648	1.473	1.380	1.557
20.5	1.604	1.647	1.485	1.403	1.560
21.0	1.602	1.643	1.499	1.428	1.566
21.5	1.600	1.637	1.513	1.452	1.572
22.0	1.593	1.629	1.526	1.473	1.575
22.5	1.587	1.619	1.531	1.487	1.575
23.0	1.578	1.608	1.532	1.492	1.572
23.5	1.570	1.596	1.530	1.494	1.564
24.0	1.560	1.581	1.527	1.495	1.555
24.5	1.547	1.565	1.519	1.493	1.545
25.0	1.532	1.547	1.511	1.488	1.533
25.5	1.517	1.529	1.500	1.479	1.518
26.0	1.501	1.508	1.485	1.468	1.500
26.5	1.480	1.486	1.468	1.458	1.482
27.0	1.460	1.465	1.447	1.435	1.459
27.5	1.438	1.439	1.424	1.415	1.436
28.0	1.414	1.414	1.402	1.393	1.411
28.5	1.387	1.387	1.376	1.371	1.387
29.0	1.360	1.360	1.351	1.347	1.359
29.5	1.330	1.330	1.323	1.322	1.330
30.0	1.300	1.300	1.294	1.293	1.300
30.5	1.267	1.267	1.264	1.263	1.267
31.0	1.231	1.231	1.229	1.229	1.231
31.5	1.195	1.195	1.194	1.195	1.195
32.0	1.158	1.158	1.158	1.158	1.158
32.5	1.118	1.118	1.118	1.118	1.118
33.0	1.076	1.076	1.076	1.076	1.076
33.5	1.031	1.031	1.031	1.031	1.031
34.0	.984	.984	.984	.984	.984
34.5	.932	.932	.932	.932	.932
35.0	.878	.878	.878	.878	.878
35.3	.8435	.8435	.8435	.8435	.8435

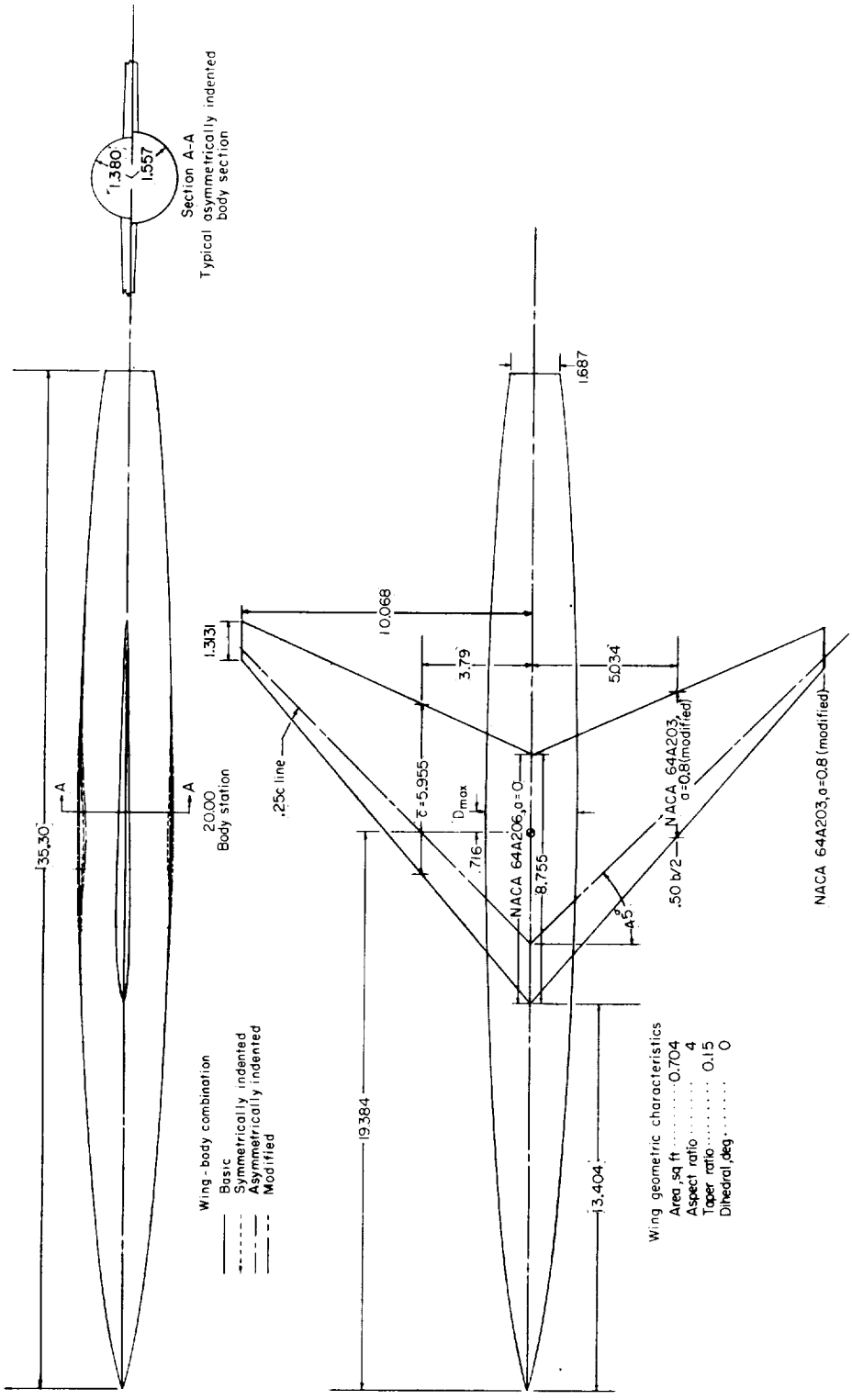

Figure 1.- Geometric characteristics of wing-body combinations used in the investigation. All dimensions are in inches.

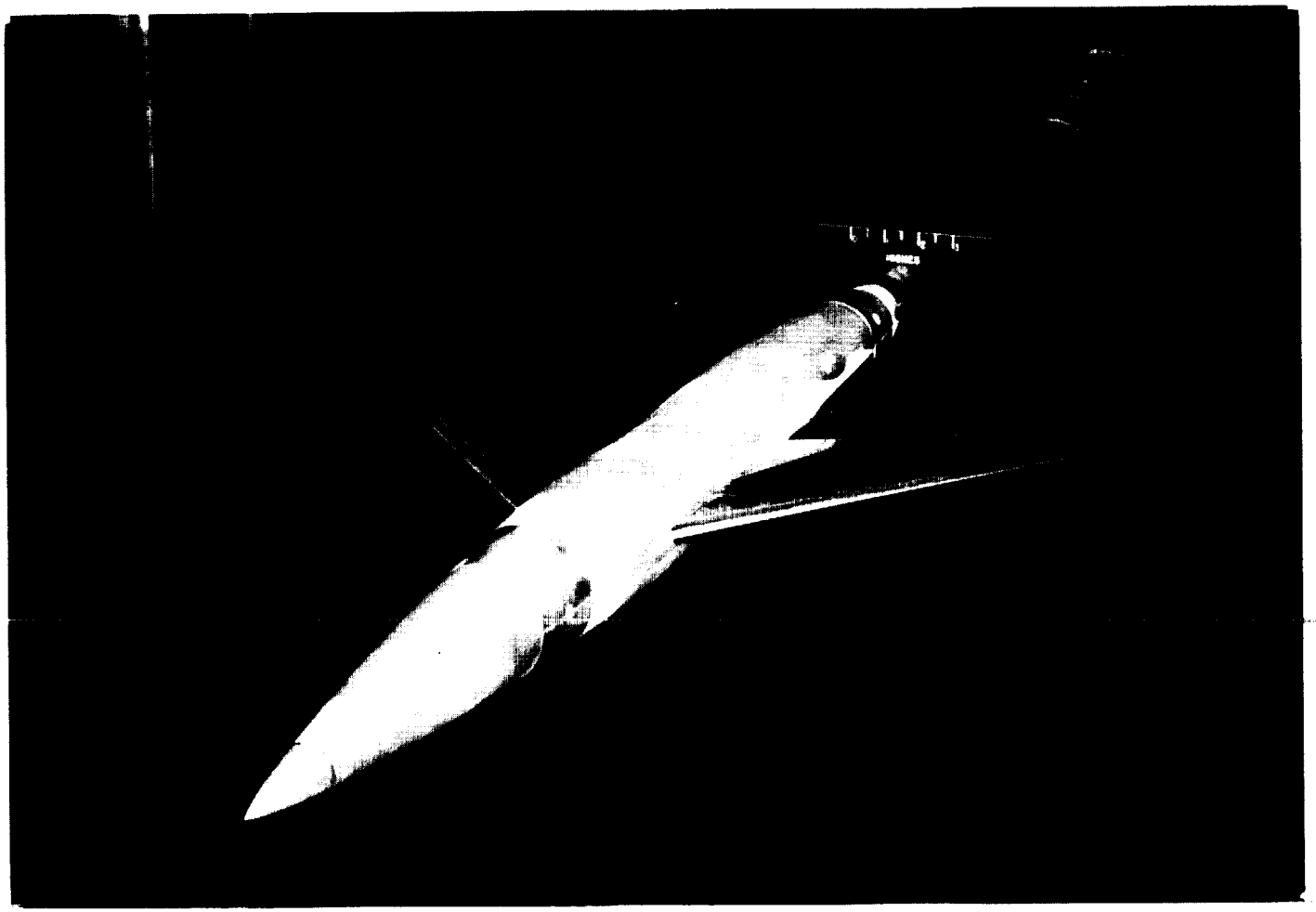

L-93027.1

Figure 2.- The 45° sweptback wing in combination with the asymmetrically indented body mounted in the Langley 8-foot transonic pressure tunnel.

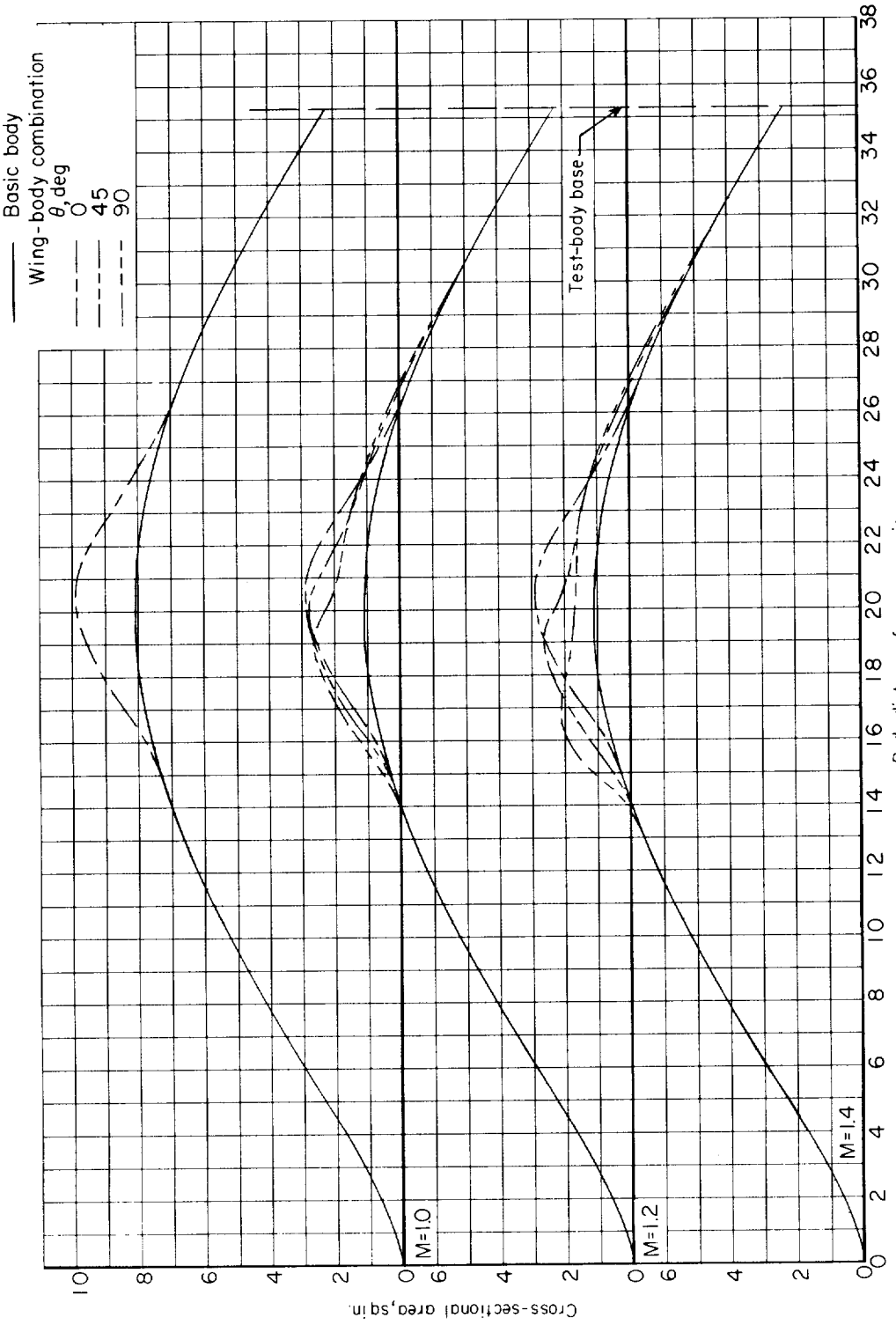

Figure 3.- Representative axial distribution of cross-sectional area for 45° sweptback wing in combination with the basic body at Mach numbers of 1.0, 1.2, and 1.4.

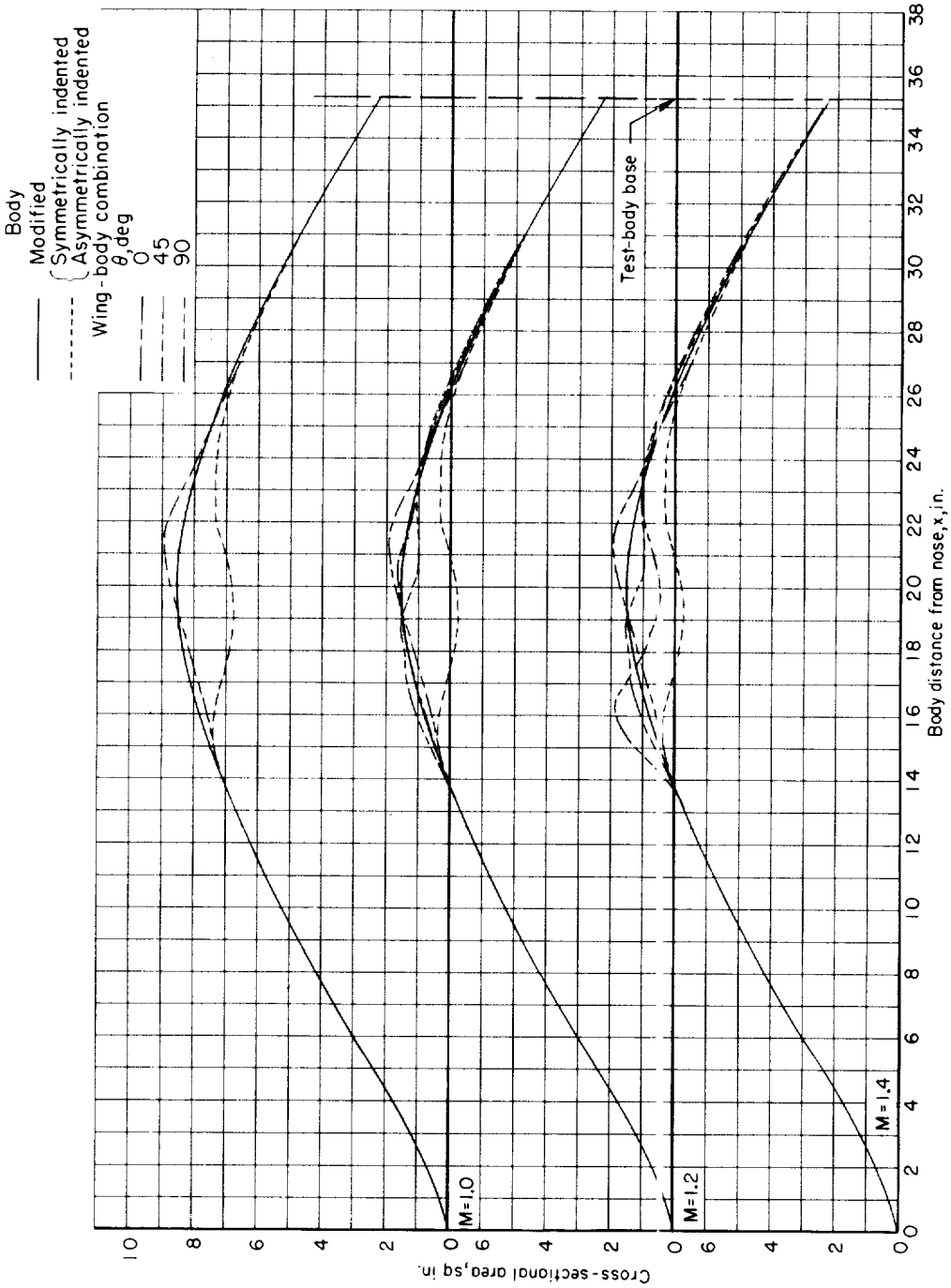

Figure 4.- Representative axial distribution of cross-sectional area for 45° sweptback wing in combination with the symmetrically indented body and the asymmetrically indented body at Mach numbers of 1.0, 1.2, and 1.4.

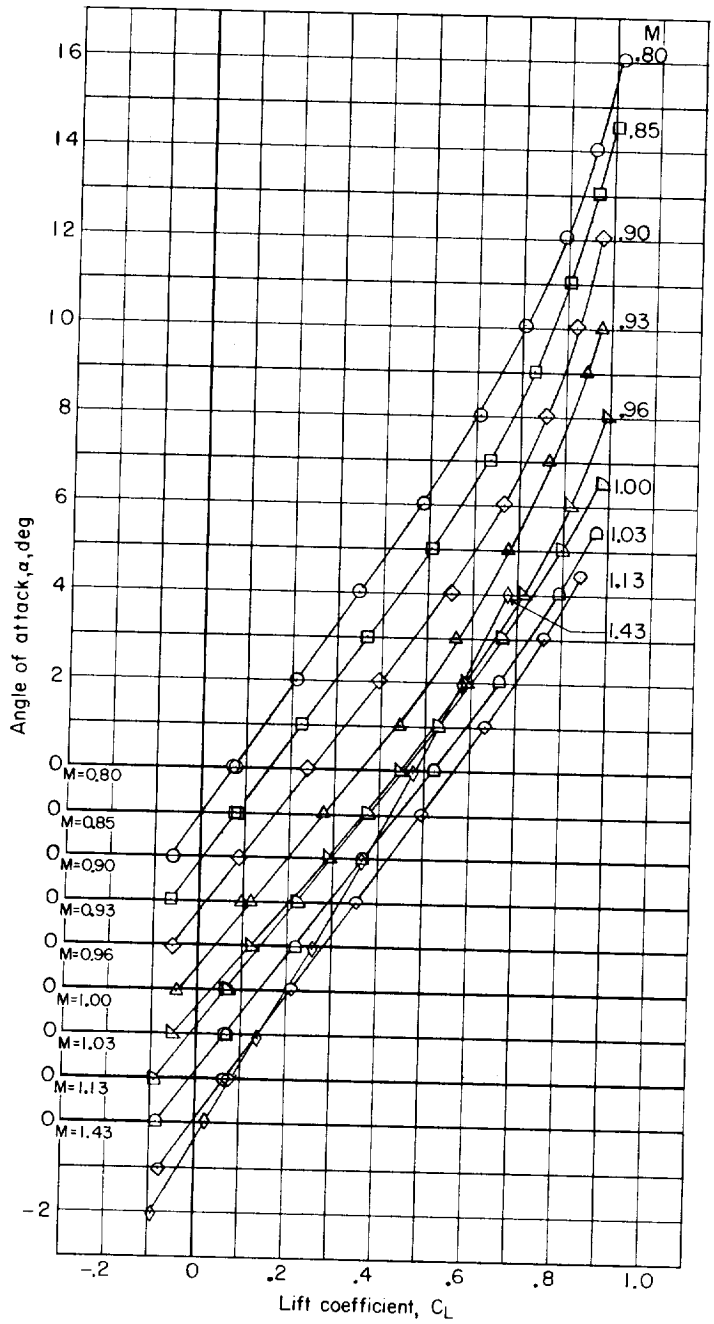

(a) α plotted against C_L for basic body configuration.

Figure 5.- Basic aerodynamic characteristics of the various wing-body combinations with transition fixed.

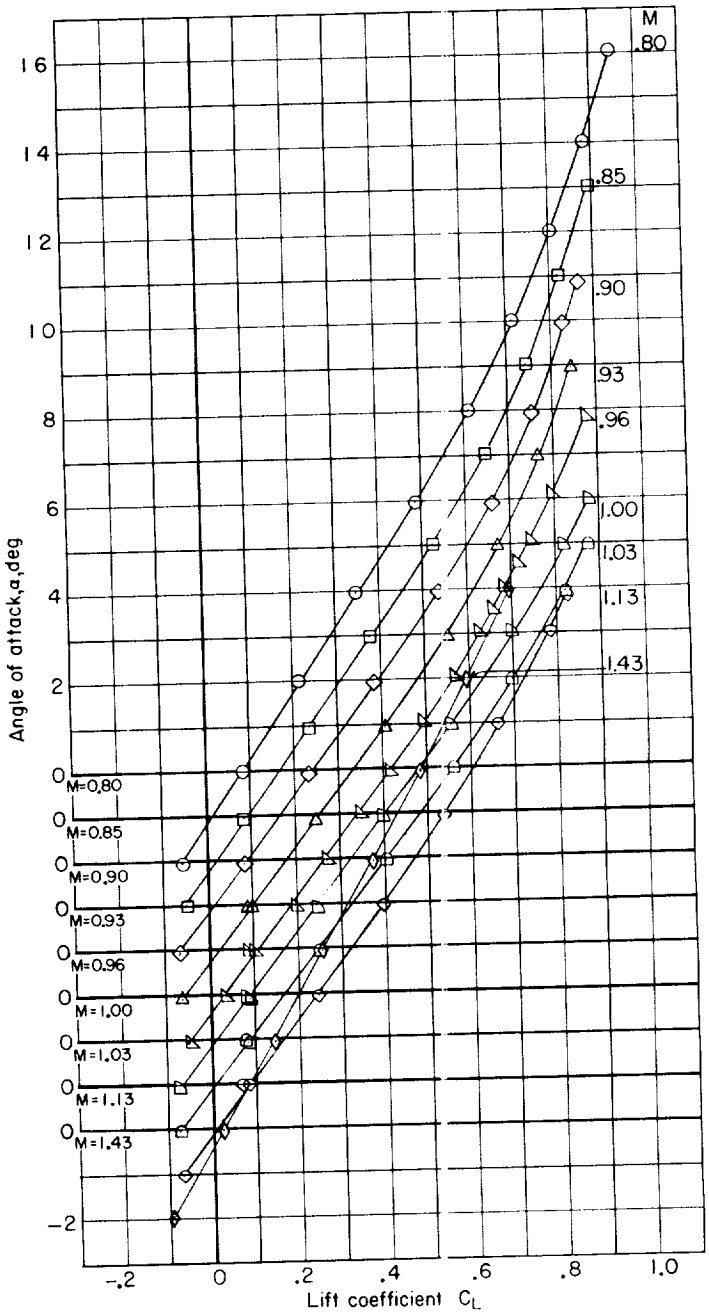

(b) α plotted against C_L for symmetrically indented body configuration.

Figure 5.- Continued.

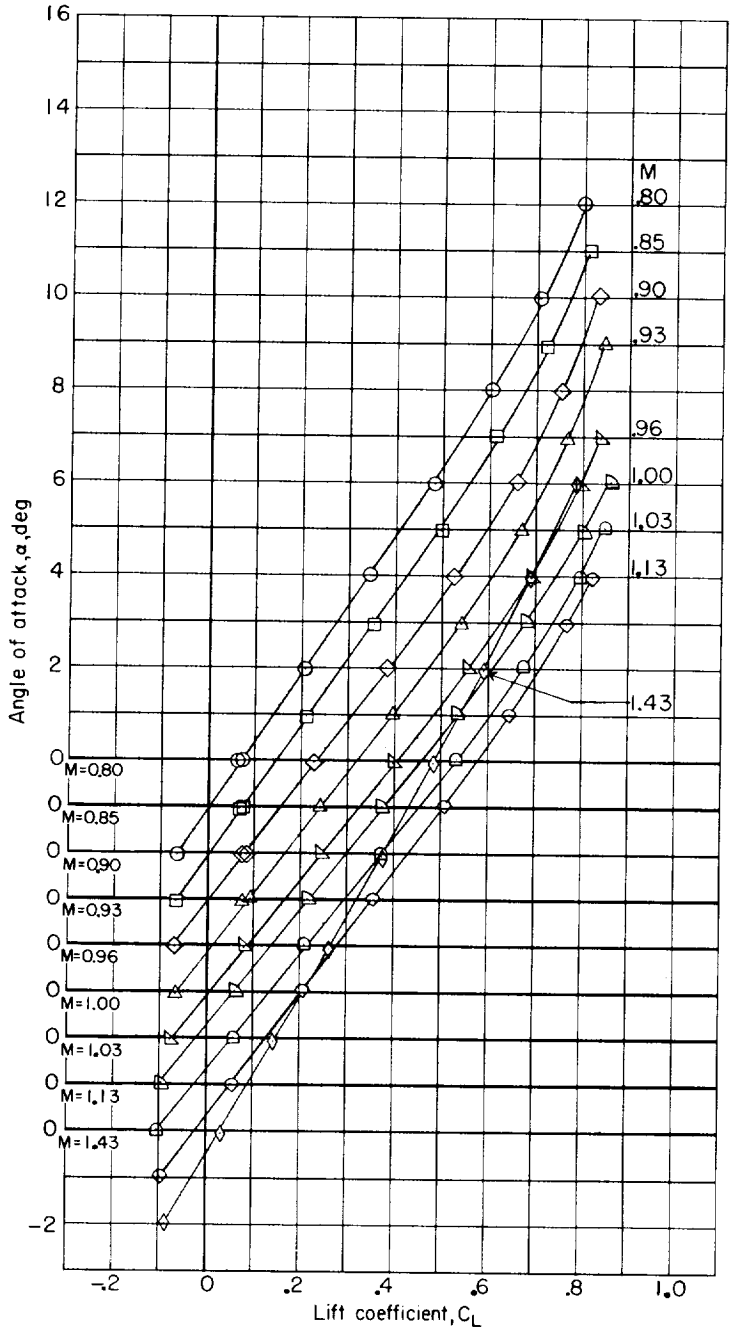

(c) α plotted against C_L for asymmetrically indented body configuration.

Figure 5.- Continued.

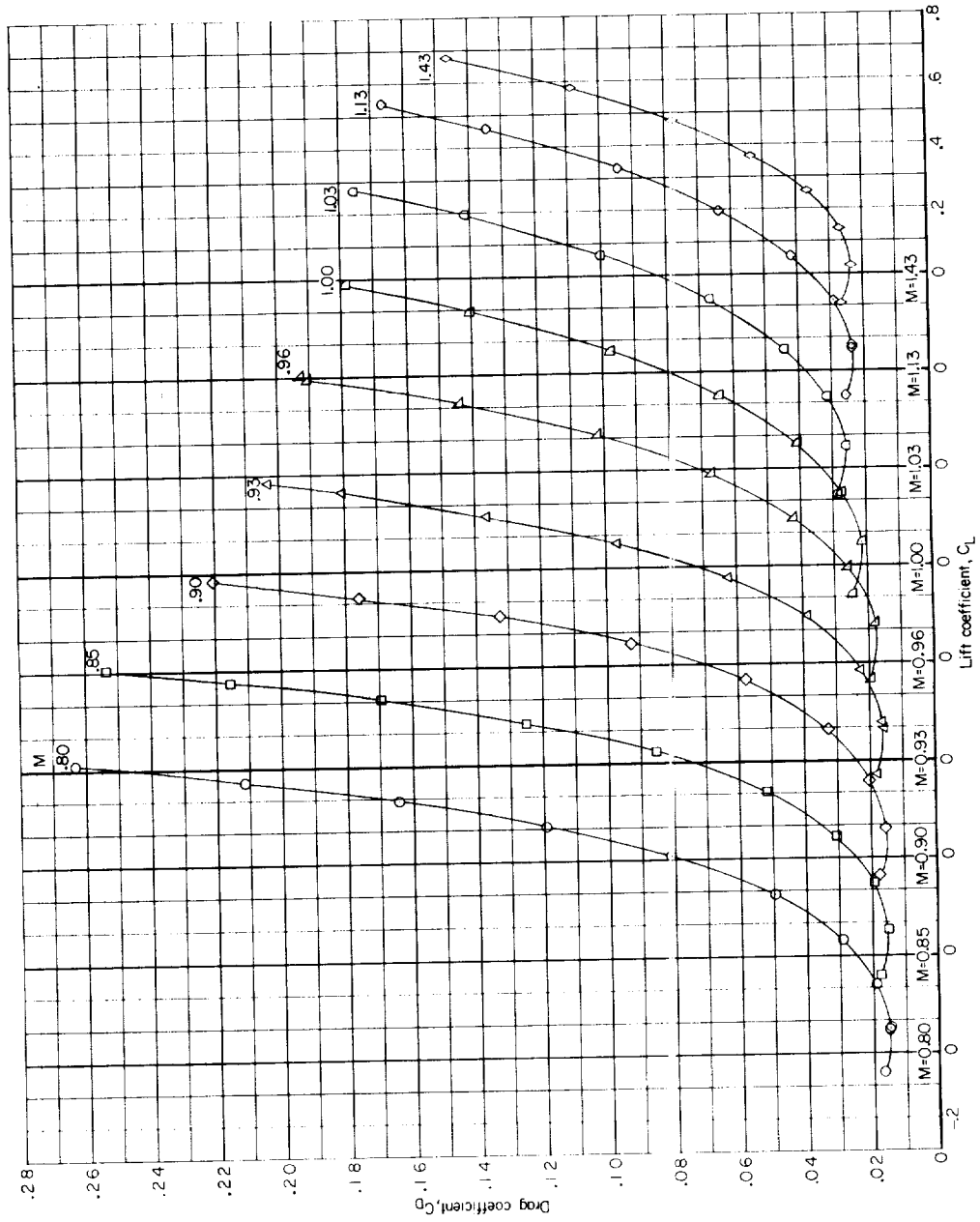

(d) C_D plotted against C_L for basic body configuration.

Figure 5.- Continued.

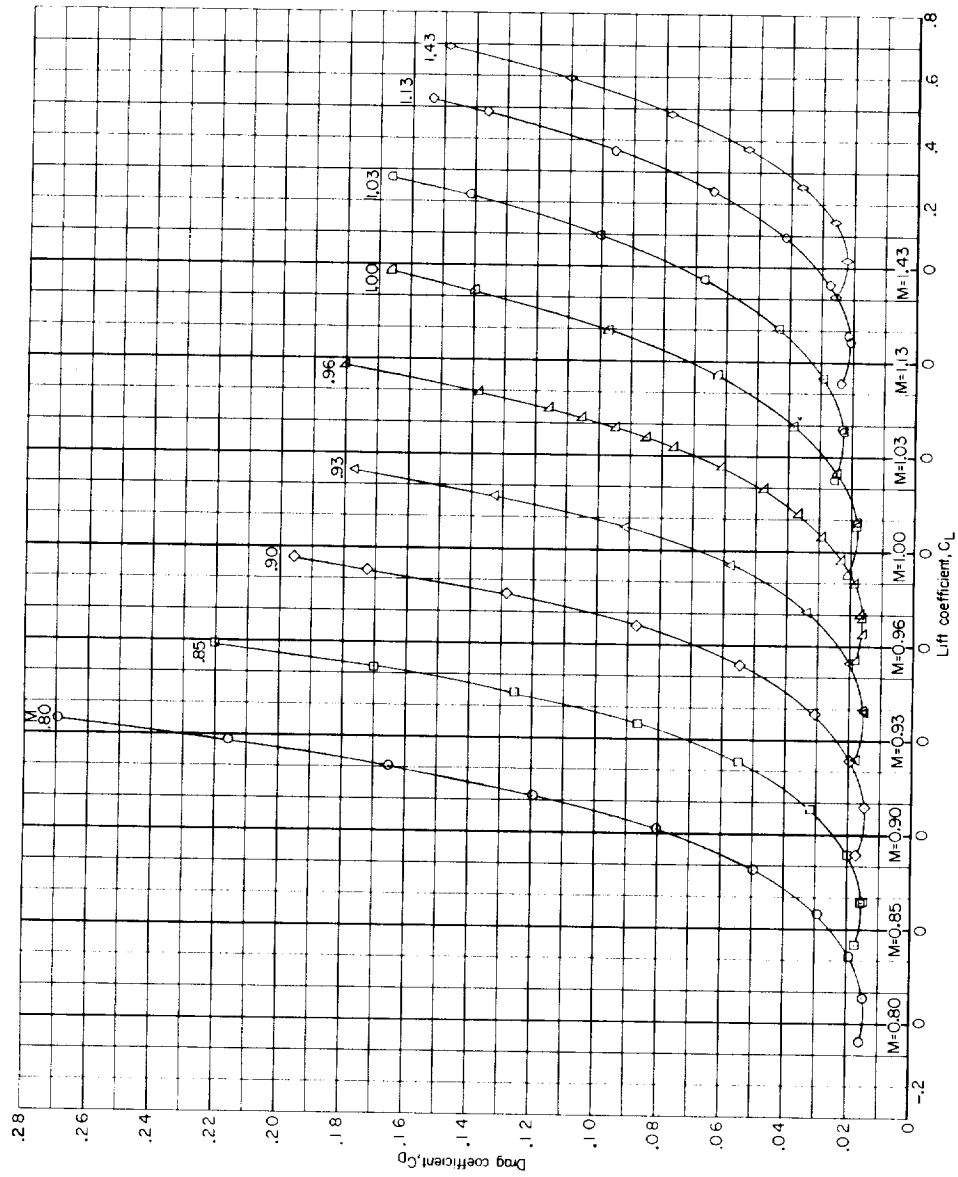

(e) C_D plotted against C_L for symmetrically indented body configuration.

Figure 5.- Continued.

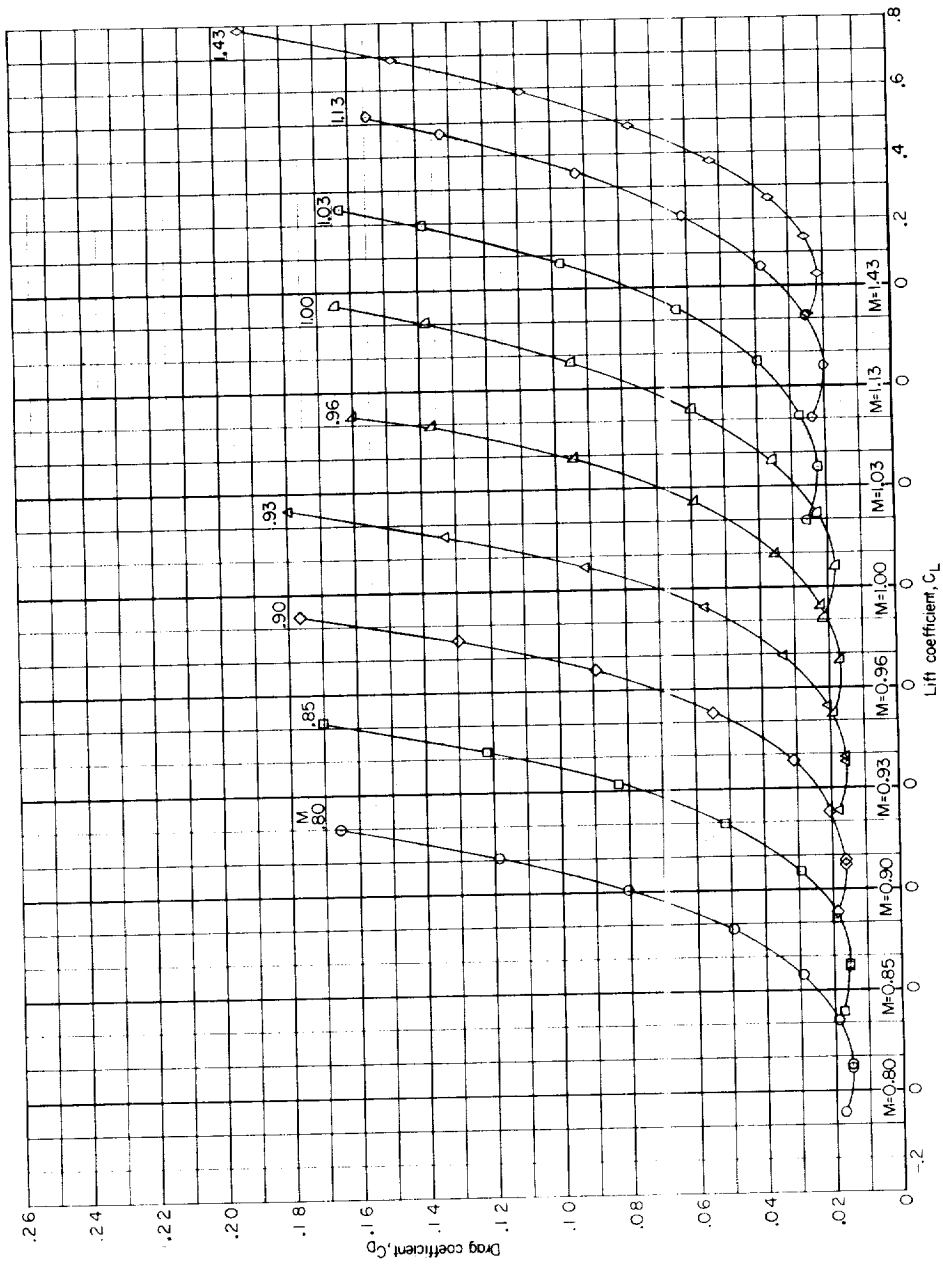

(f) C_D plotted against C_L for asymmetrically indented body configuration.

Figure 5.- Continued.

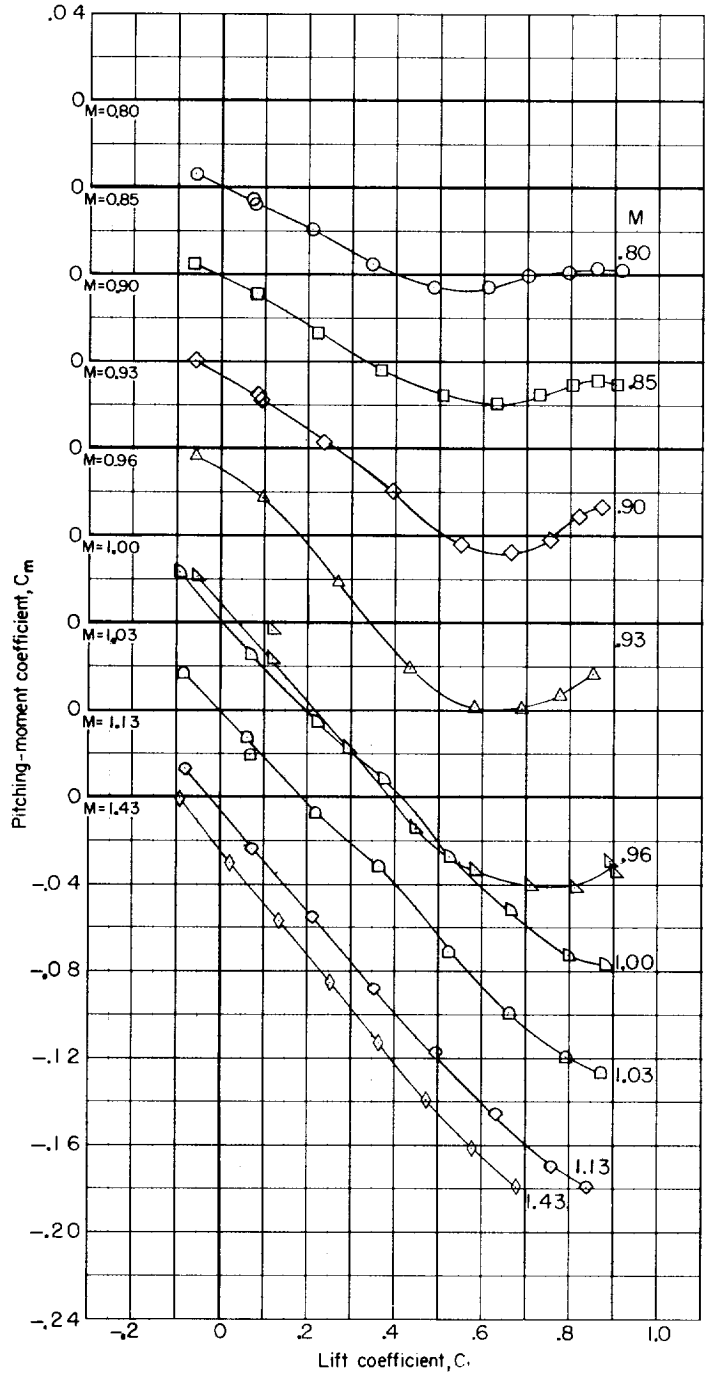

(g) C_m plotted against C_L for basic body configuration.

Figure 5.- Continued.

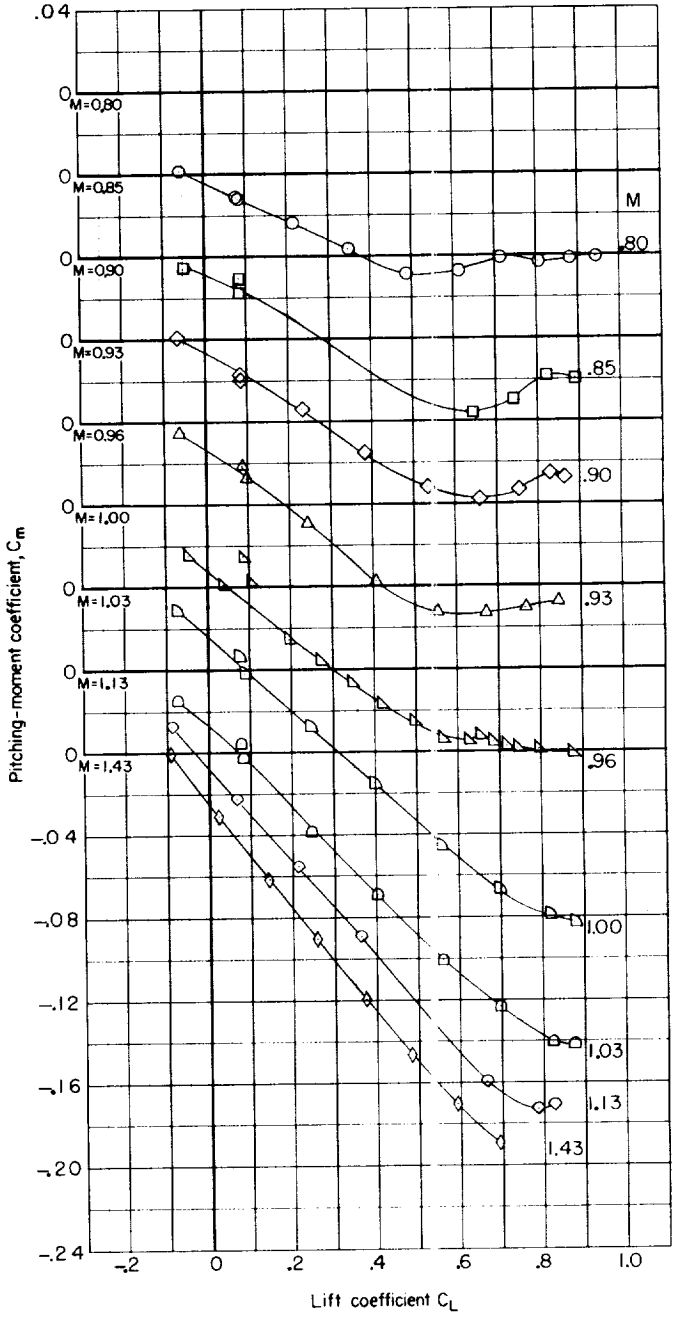

(h) C_m plotted against C_L for symmetrically indented body configuration.

Figure 5.- Continued.

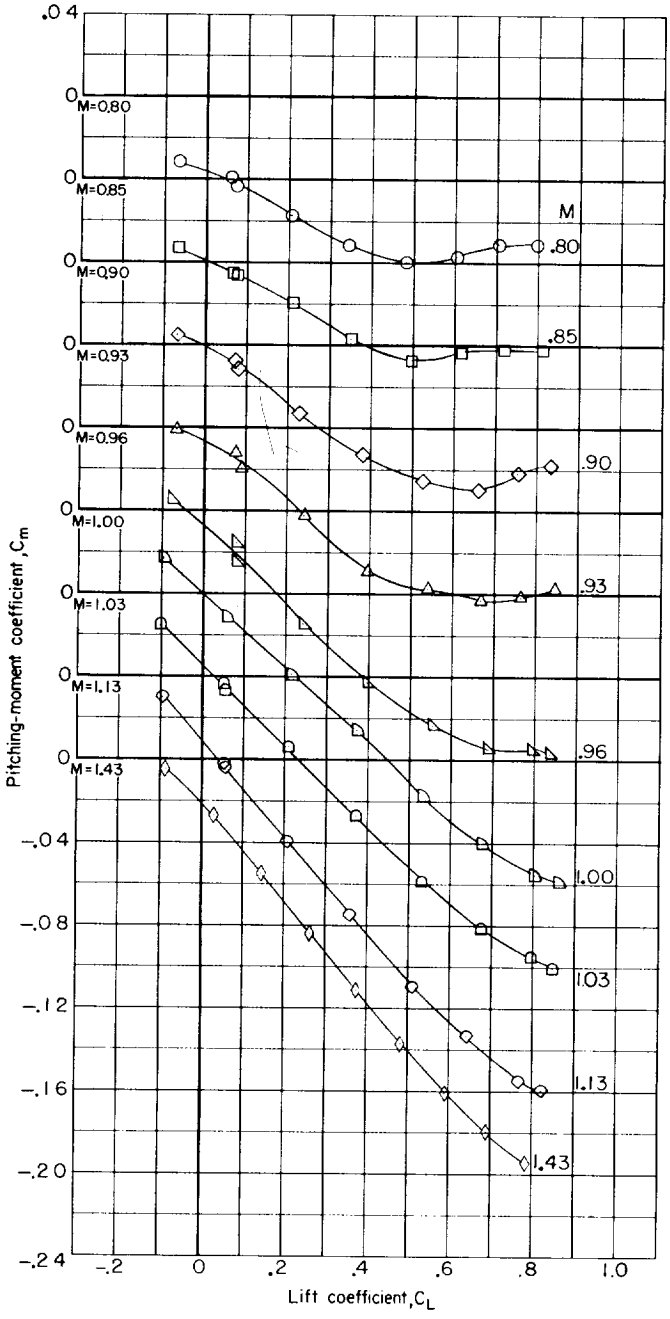

(i) C_m plotted against C_L for asymmetrically indented body configuration.

Figure 5.- Concluded.

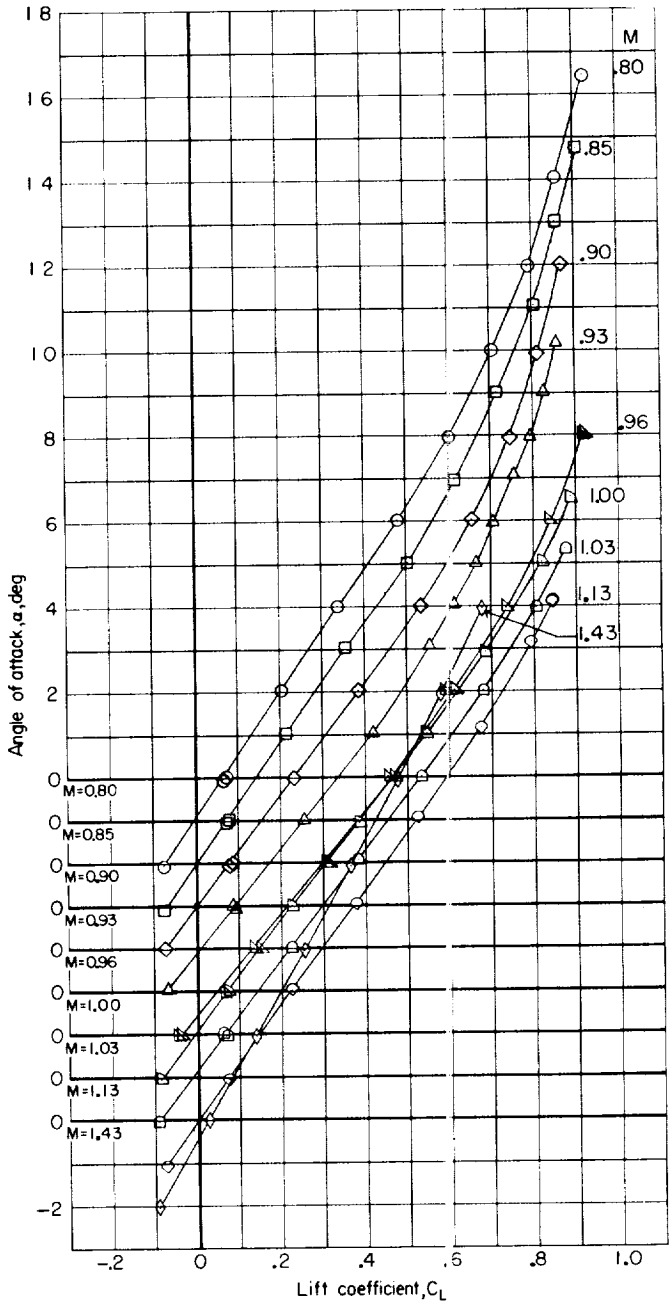

(a) α plotted against C_L for basic body configuration.

Figure 6.- Basic aerodynamic characteristics of the various wing-body combinations with transition natural.

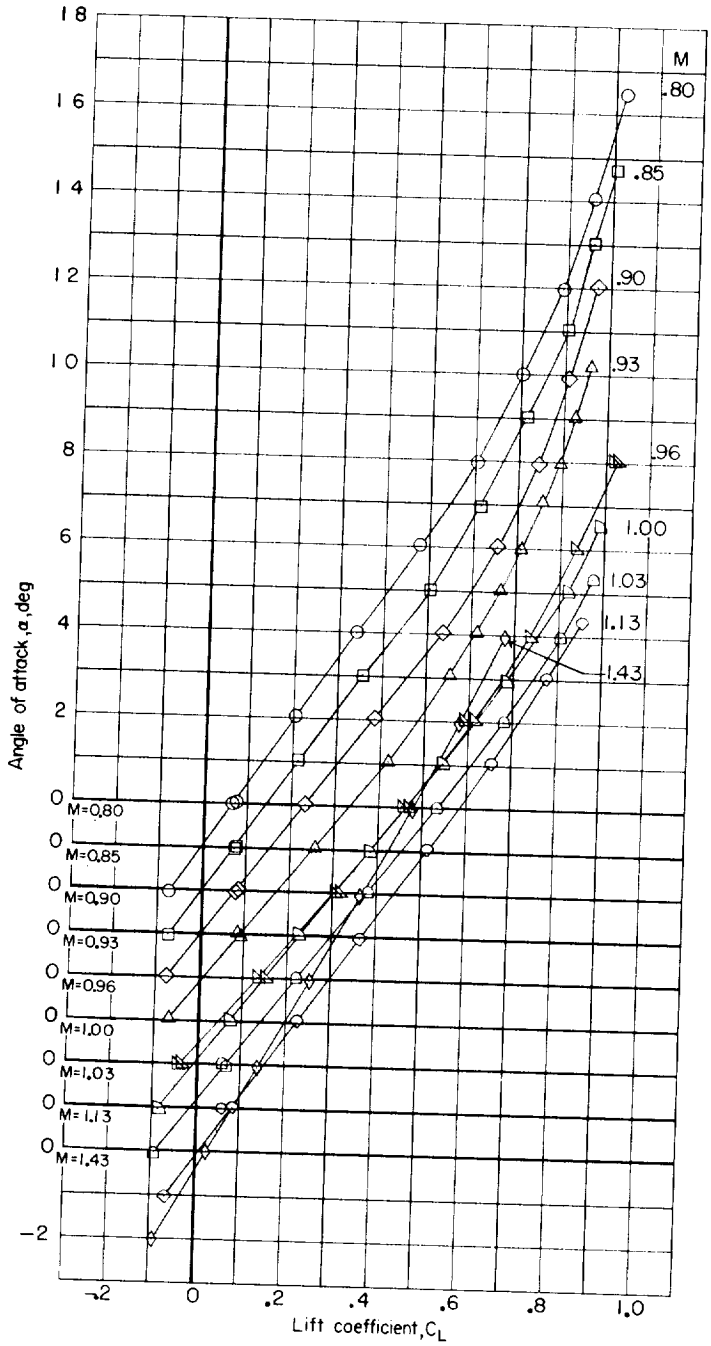

(b) α plotted against C_L for symmetrically indented body configuration.

Figure 6.- Continued.

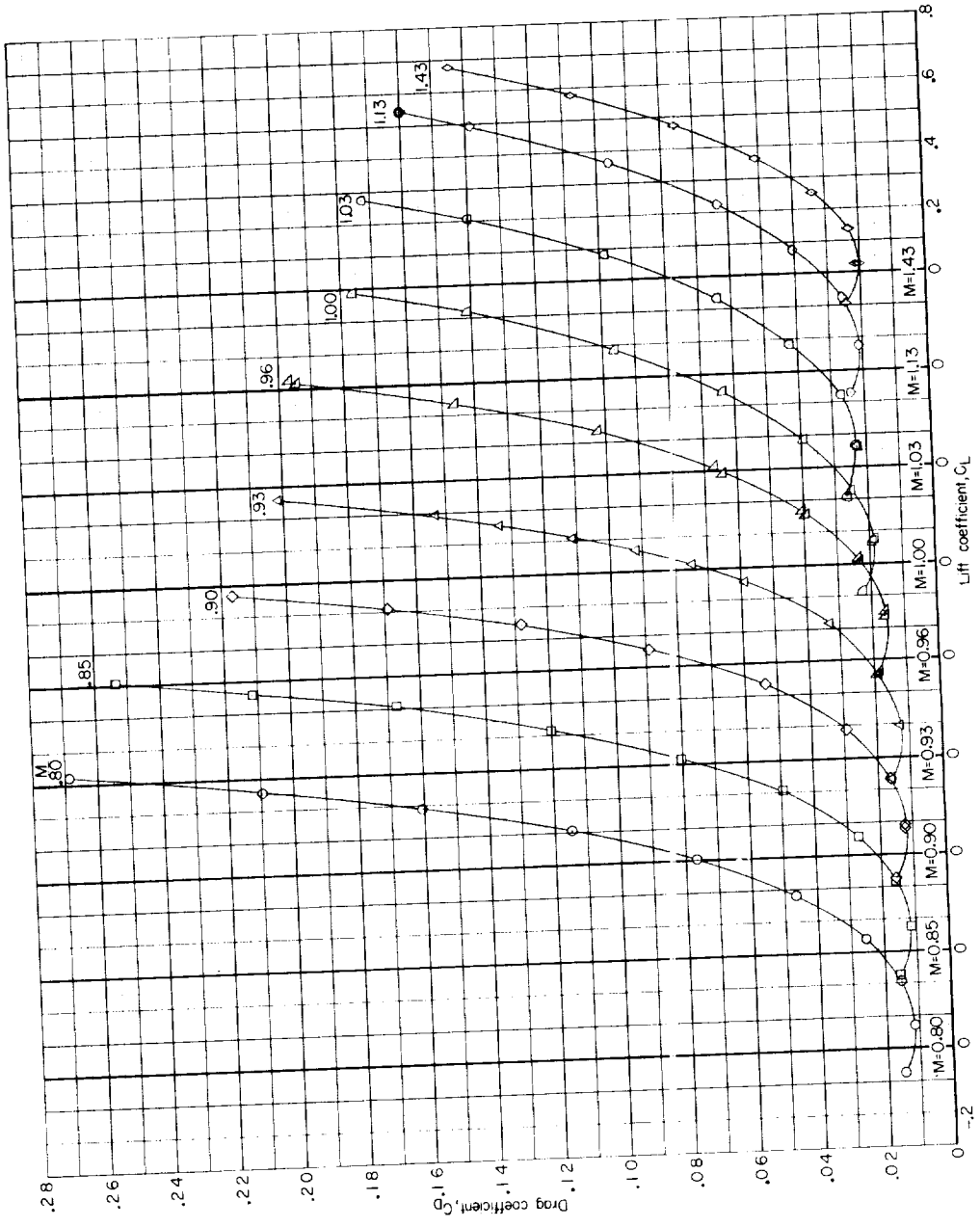

(c) C_D plotted against C_L for basic body configuration.

Figure 6.- Continued.

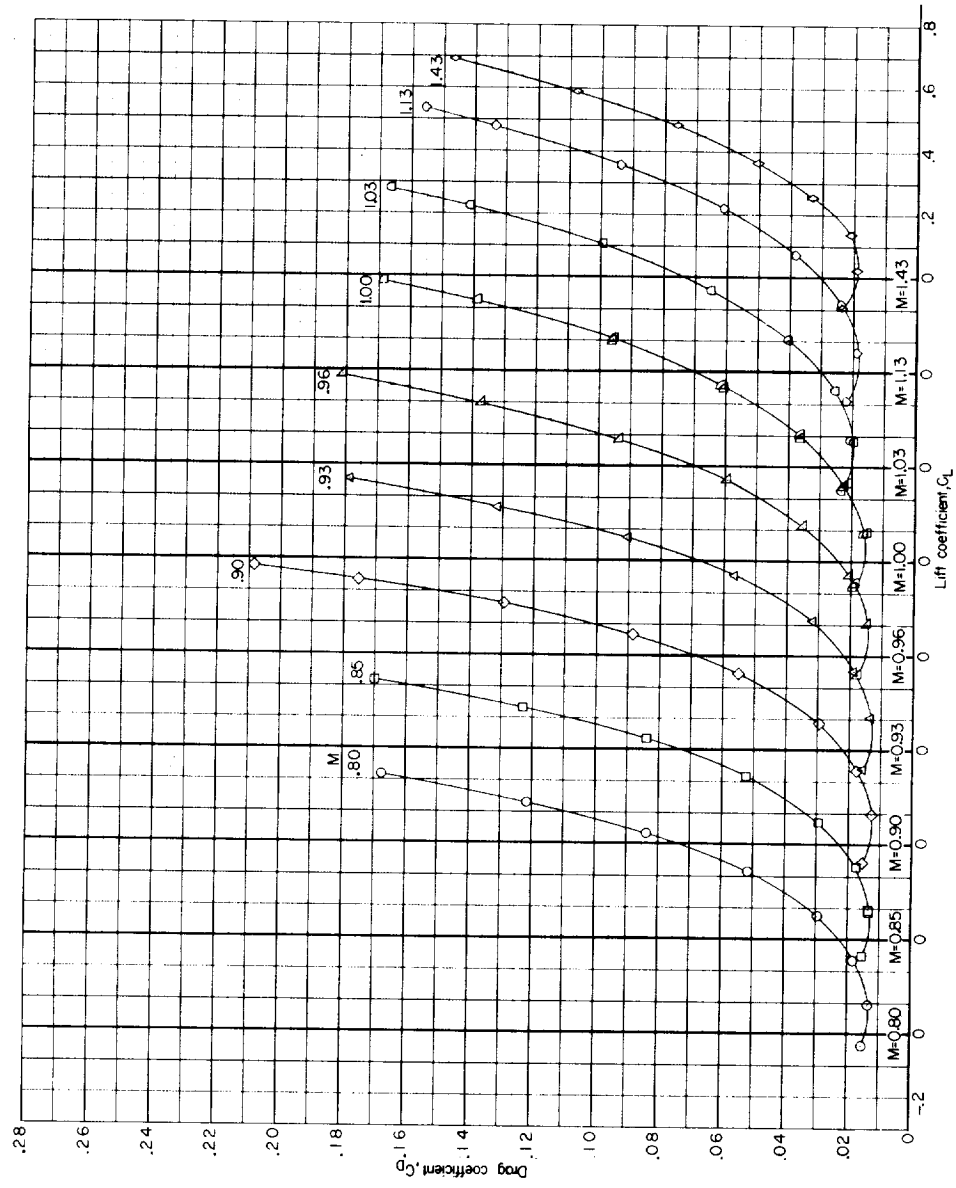

(d) C_D plotted against C_L for symmetrically indented body configuration.

Figure 6.- Continued.

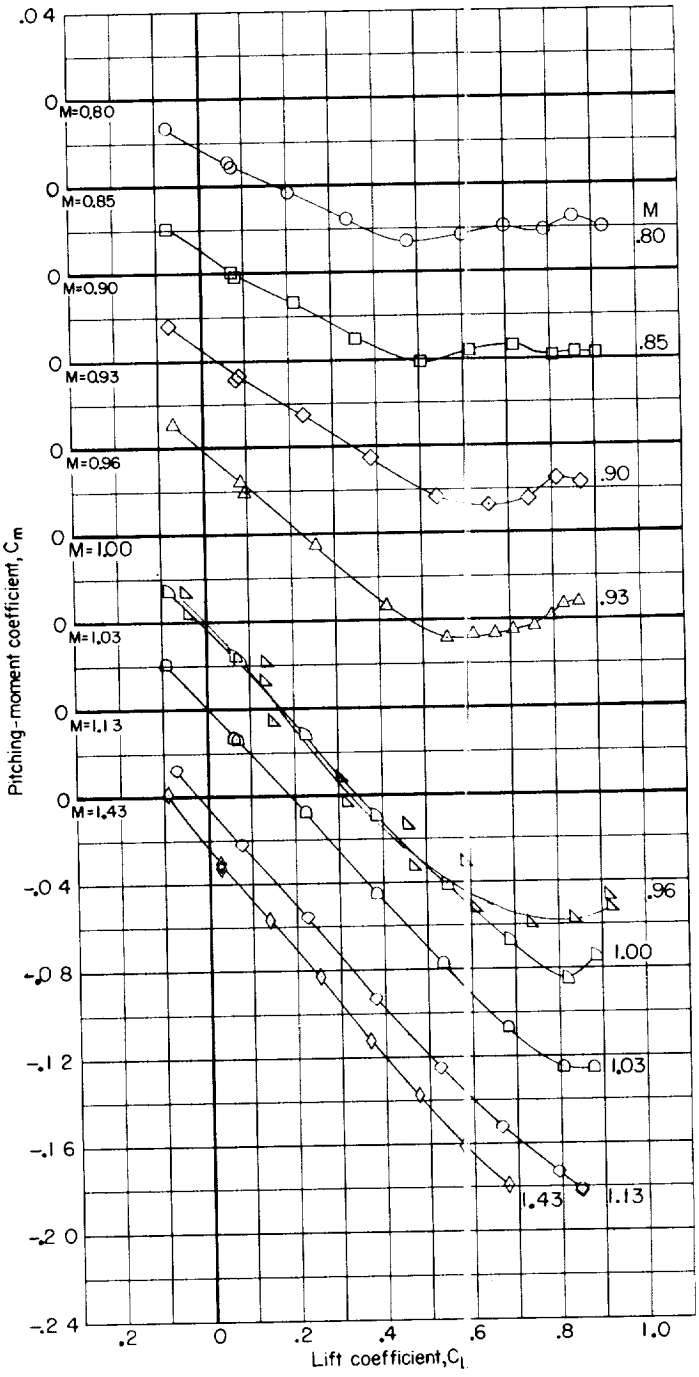

(e) C_m plotted against C_L for basic body configuration.

Figure 6.- Continued.

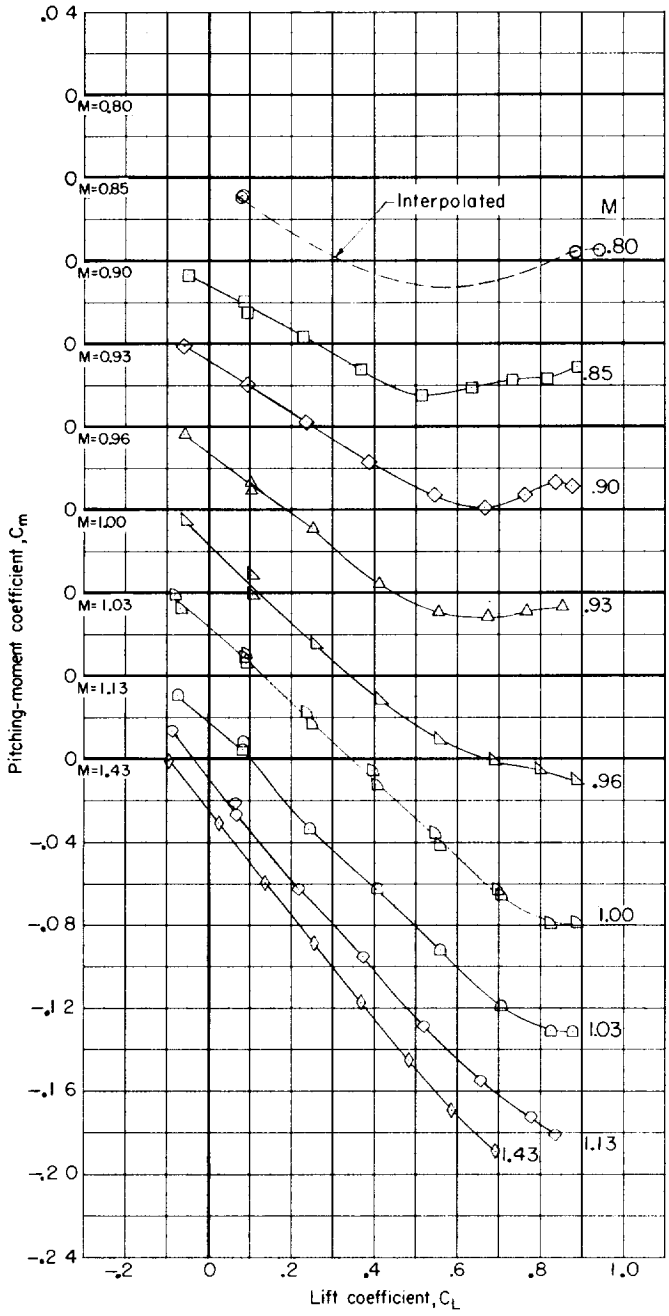

(f) C_m plotted against C_L for symmetrically indented body configuration.

Figure 6.- Concluded.

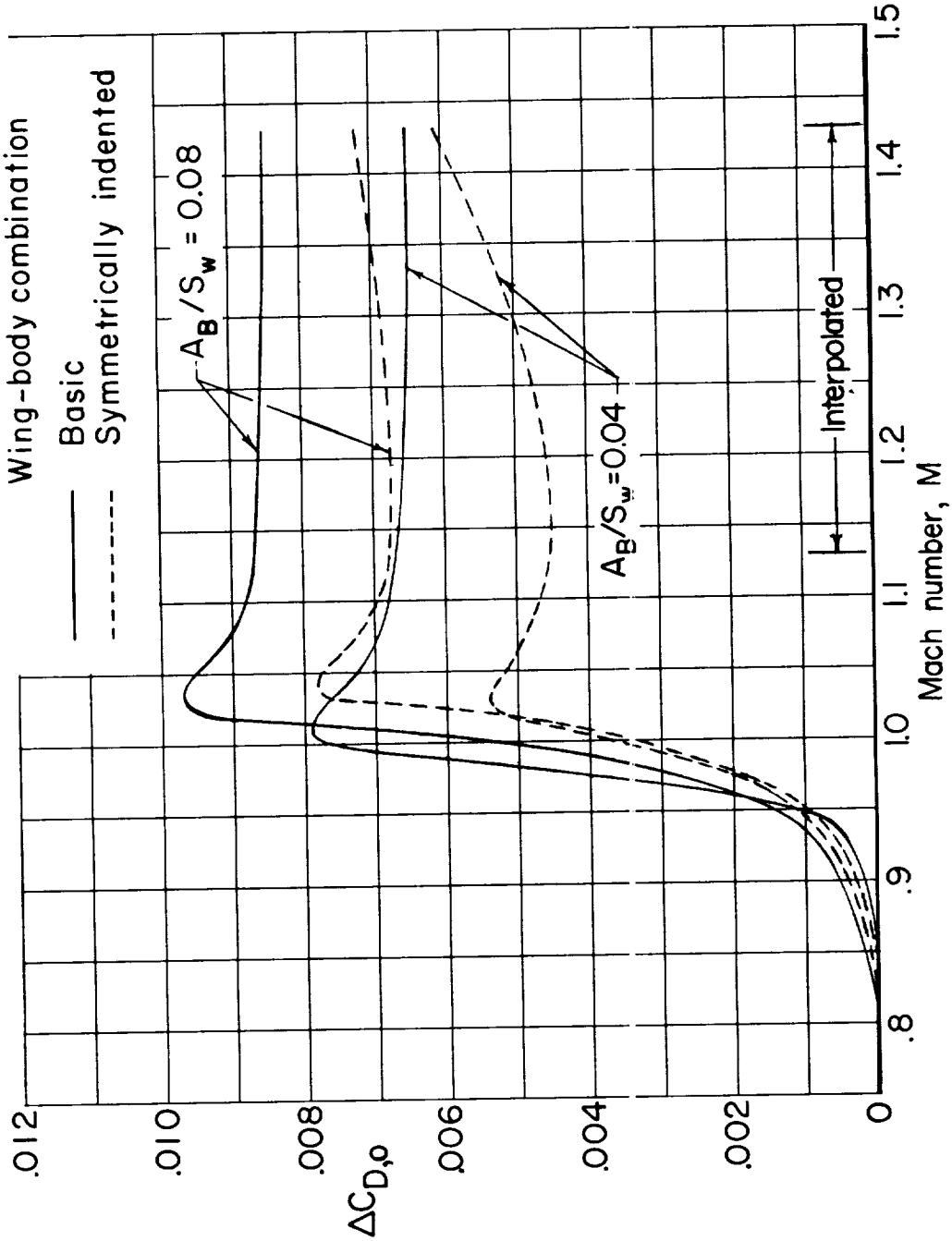

Figure 7.- Effect of relative body size on zero-lift wave-drag coefficient.

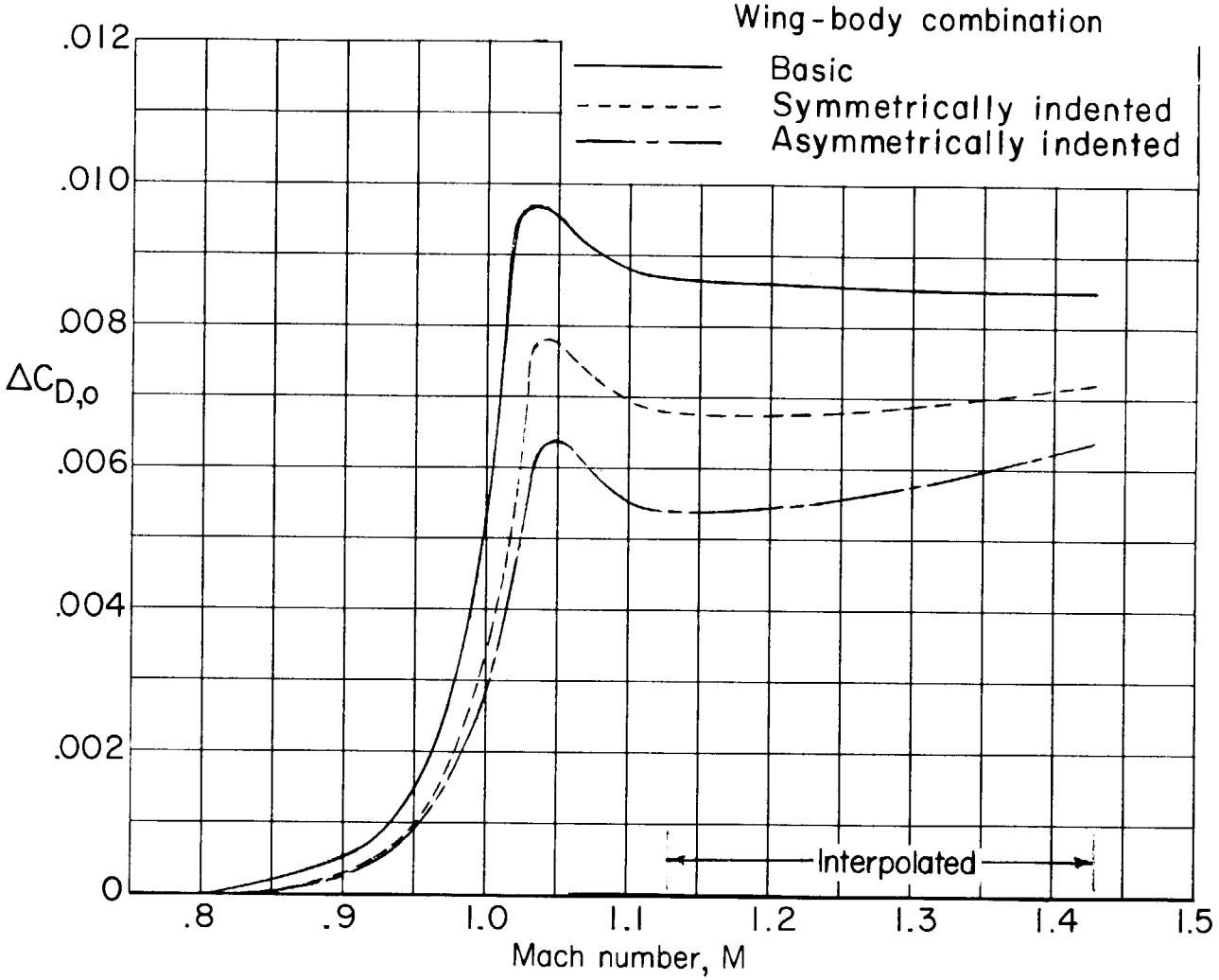

Figure 8.- Effect of symmetrical indentation and asymmetrical indentation on zero-lift wave-drag coefficient. $A_B/S_W = 0.08$.

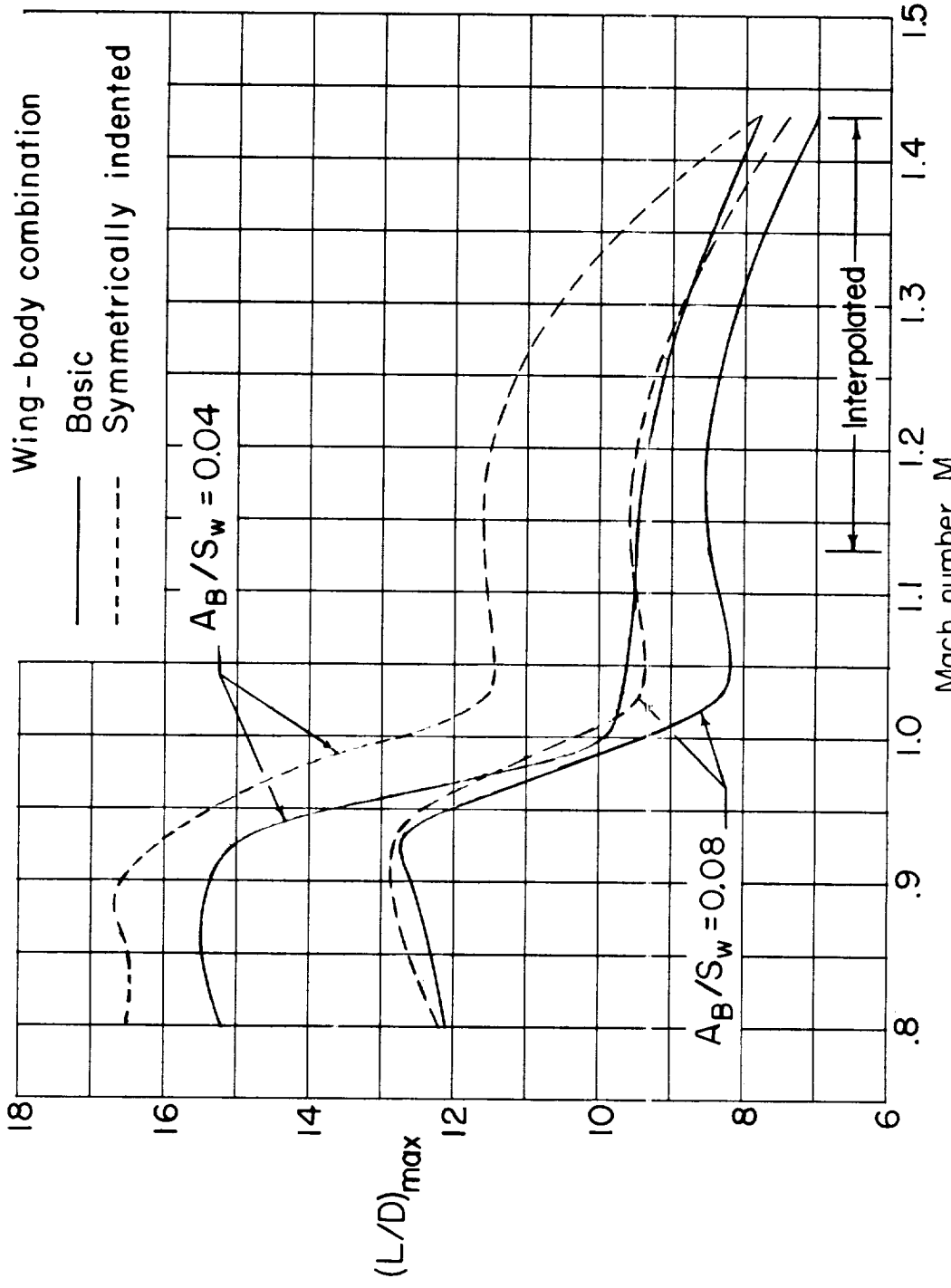

Figure 9.- Effect of relative body size on maximum lift-drag ratio.

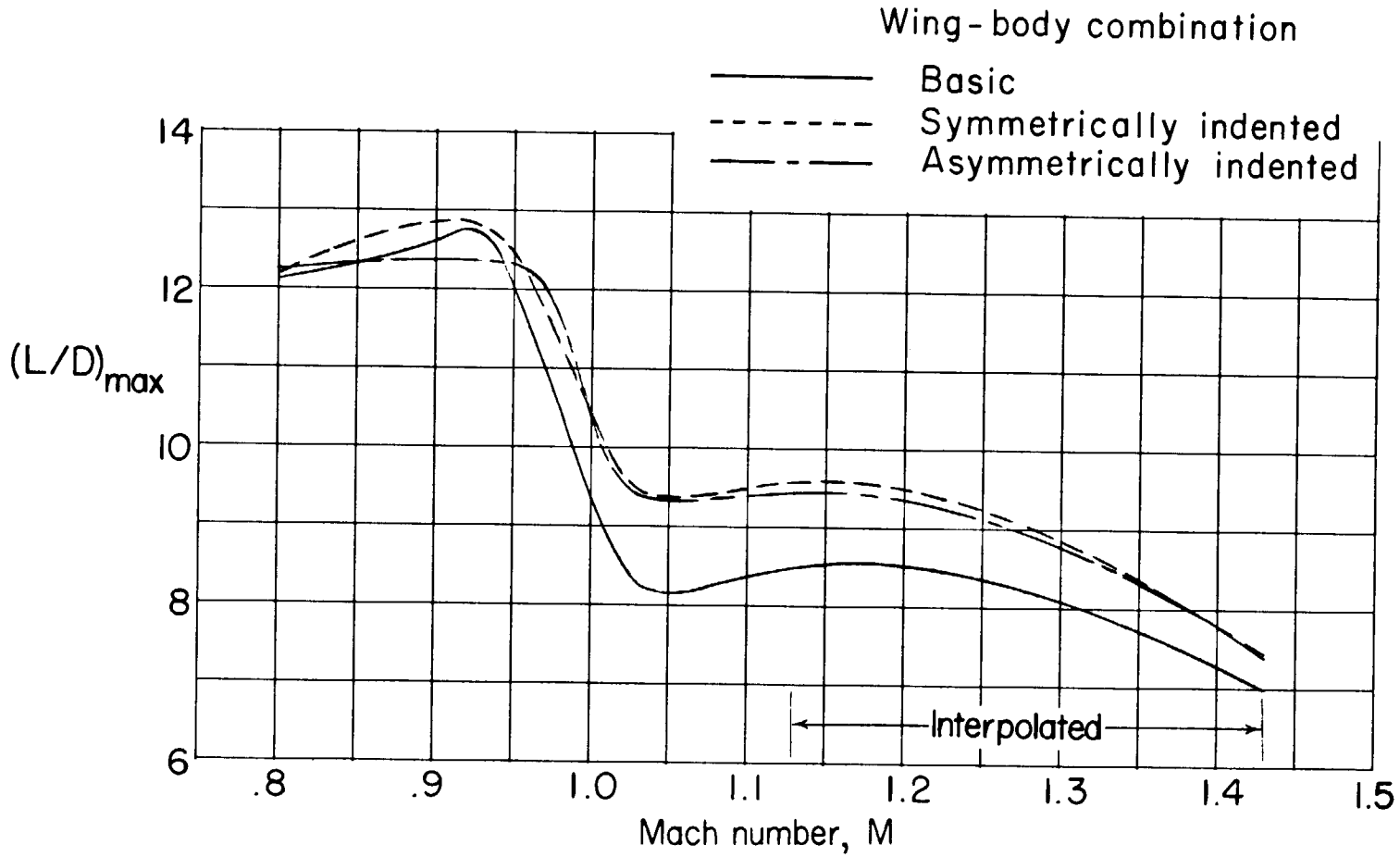

Figure 10.- Effect of symmetrical indentation and asymmetrical indentation on maximum lift-drag ratio. $A_B/S_w = 0.08$.

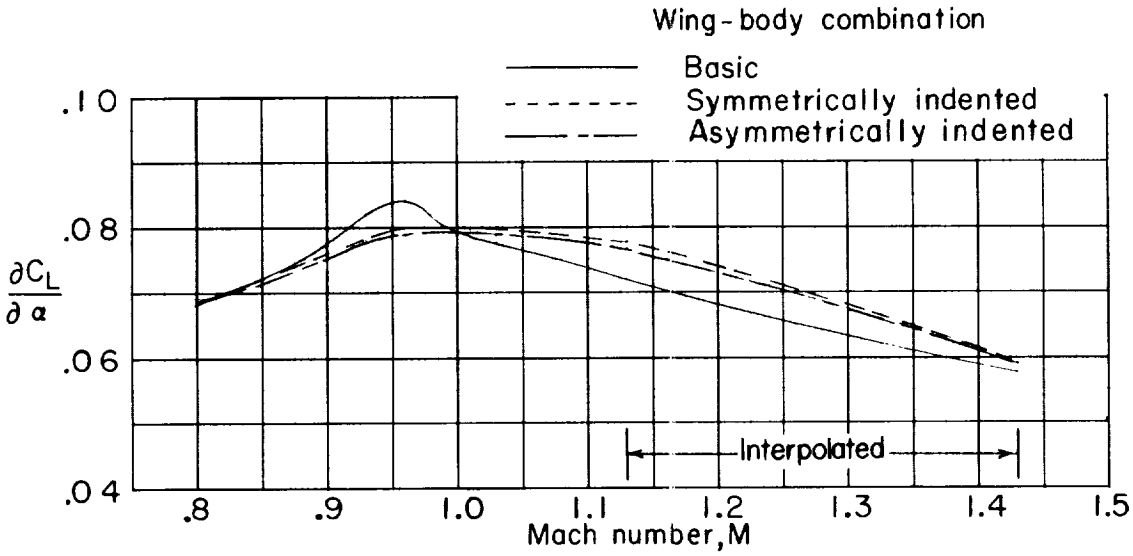

Figure 11.- Average lift-curve-slope characteristics of the 45° sweptback wing in combination with the basic and indented bodies. C_L = -0.05 to 0.3.

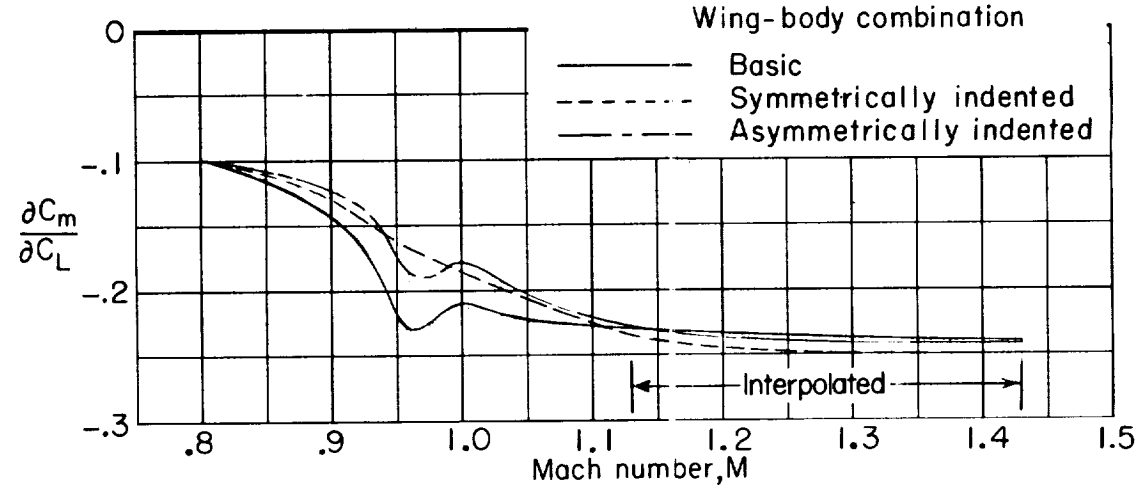

Figure 12.- Stability characteristics of the 45° sweptback wing in combination with the basic and indented bodies. C_L = -0.05 to 0.3.

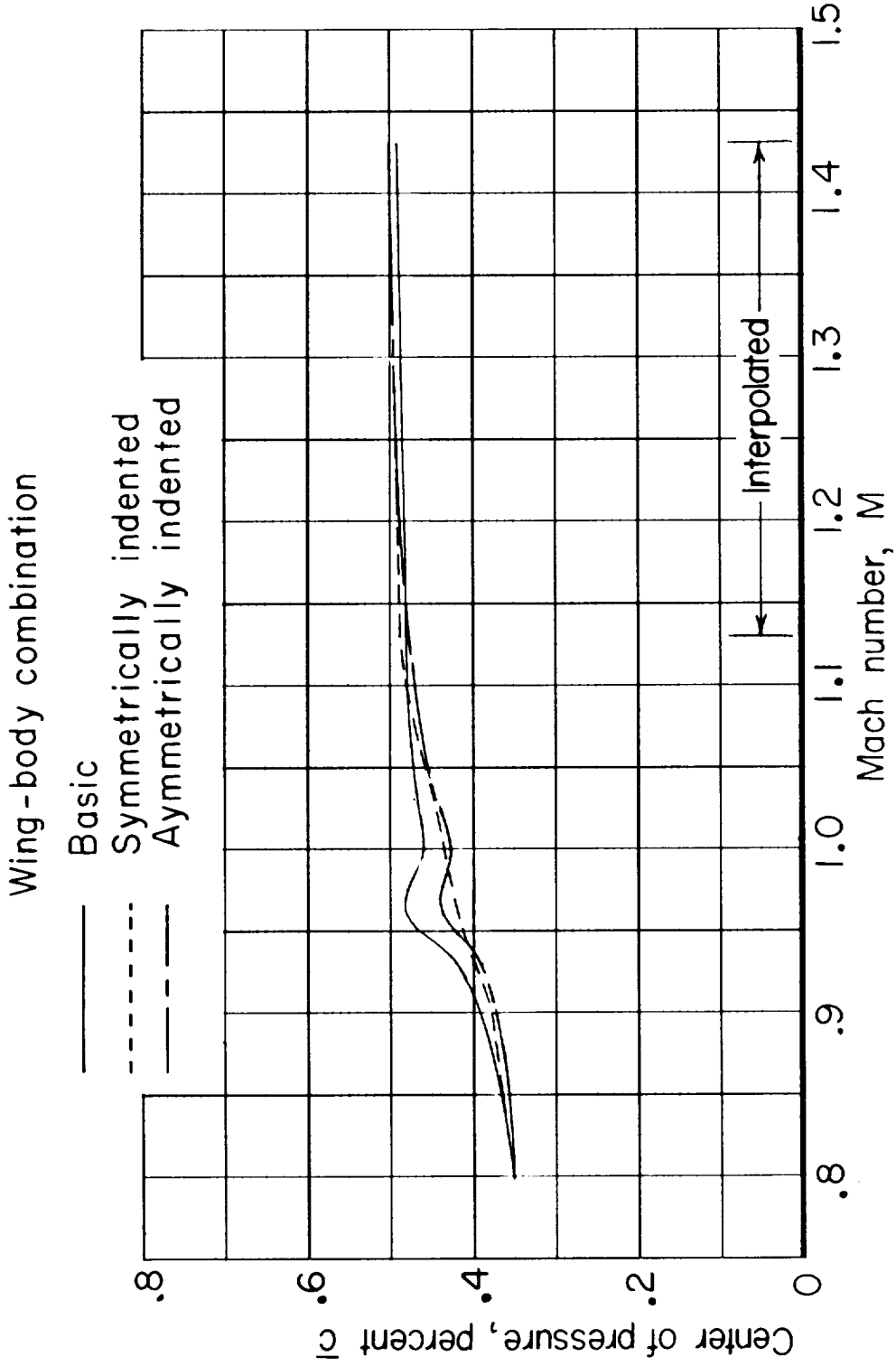

Figure 13.- Variation of the center of pressure with Mach number for the 45° sweptback wing in combination with the basic and indented bodies. C_L = -0.05 to 0.3.

NASA - Langley Field, Va. L-303